AGU PUBLICATIONS

Journal of Advances in Modeling Earth Systems

RESEARCH ARTICLE

10.1002/2015MS000480

Kinetic energy-conserving hyperdiffusion can improve low resolution atmospheric models

Pablo Zurita-Gotor[1,2], Isaac M. Held[3], and Malte F. Jansen[4]

[1]Departamento de Geofísica y Meteorología, Universidad Complutense, Madrid, Spain, [2]Instituto de Geociencia UCM-CSIC, Madrid, Spain, [3]NOAA Geophysical Fluid Dynamics Laboratory, Princeton, New Jersey, [4]Department of the Geophysical Sciences, The University of Chicago, Chicago, Illinois

Key Points:
- Strong subgrid dissipation may degrade low resolution atmospheric simulations
- A kinetic energy-conserving scheme gives better results, even at moderate resolutions
- Sensitivity to damping rate is reduced with the kinetic energy-conserving scheme

Correspondence to:
P. Zurita-Gotor,
pzurita@alum.mit.edu

Citation:
Zurita-Gotor, P., I. M. Held, and M. F. Jansen (2015), Kinetic energy-conserving hyperdiffusion can improve low resolution atmospheric models, *J. Adv. Model. Earth Syst.*, *7*, 1117–1135, doi:10.1002/2015MS000480.

Received 4 MAY 2015
Accepted 2 JUL 2015
Accepted article online 8 JUL 2015
Published online 25 JUL 2015

Abstract Motivated by findings that energetically consistent subgrid dissipation schemes can improve eddy-permitting ocean simulations, this work investigates the impact of the subgrid dissipation scheme on low-resolution atmospheric dynamical cores. A kinetic energy-conserving dissipation scheme is implemented in the model adding a negative viscosity term that injects back into the eddy field the kinetic energy dissipated by horizontal hyperdiffusion. The kinetic energy-conserving scheme enhances numerical convergence when horizontal resolution is changed with fixed vertical resolution and gives superior low-resolution results. Improvements are most obvious for eddy kinetic energy but also found in other fields, particularly with strong or little scale-selective horizontal hyperdiffusion. One advantage of the kinetic energy-conserving scheme is that it reduces the sensitivity of the model to changes in the subgrid dissipation rate, providing more robust results.

1. Introduction

The vast expansion of computational power has fostered great advances in atmospheric modeling, so that global cloud-resolving simulations are becoming possible for short integrations [*Sato et al.*, 2009] and coupled climate models can now be run at atmospheric resolutions of 1° or less [*Delworth et al.*, 2012; *Shaffrey et al.*, 2009]. Yet at the same time atmospheric resolution still poses a constraint for very long transient or equilibrated integrations, as needed for instance in the context of paleoclimate studies [e.g., *Liu et al.*, 2009]. Simulations with Earth System Models spanning thousands of years often need to rely on reduced or statistical atmospheric models [*Timm and Timmerman*, 2007; *Montoya et al.*, 2005], or employ atmospheric dynamical cores with limited horizontal resolution [*Shields et al.*, 2012; *Smith and Gregory*, 2012]. Thus, even as atmospheric models achieve unprecedented resolutions there is still a practical interest in constructing robust and efficient low-resolution atmospheric models.

The minimum requirement that a low-resolution atmospheric model should satisfy is to produce extratropical stormtracks with eddies of realistic amplitude. With too coarse resolution, the circulation of a model and its sensitivity to external forcing are marred by the weak eddy activity. This is a similar difficulty as currently encountered by "eddy-permitting" ocean circulation models, which can produce some eddy activity but are still too coarse to fully resolve the eddies [*Hallberg*, 2013]. At these low resolutions the choice of subgrid scale dissipation may have dramatic effects.

Subgrid dissipation is needed to dissipate the small scale enstrophy generated by geostrophic turbulence [*Charney*, 1971], which would otherwise accumulate at the grid scale. This dissipation is typically included in the models using scale-selective hyperdiffusion so as to minimize the damping on the large scale (see *Jablonowski and Williamson* [2011] for a recent review). The problem is that at grid sizes not much finer than the deformation radius some impact on the eddies is unavoidable. In the atmosphere, much of the small-scale enstrophy is produced in association with critical layers. Because the qualitative behavior of these layers is sensitive to damping [see e.g., *Held and Phillips*, 1987], the strength of subgrid dissipation may also affect the propagation of the waves and their interaction with the mean flow.

To illustrate the impact of subgrid dissipation Figure 1 shows snapshots of upper level absolute vorticity at various resolutions and with different forms of dissipation in atmospheric simulations using the Held and Suarez benchmark [*Held and Suarez*, 1994, HS94 hereafter, model specifics are described in the next

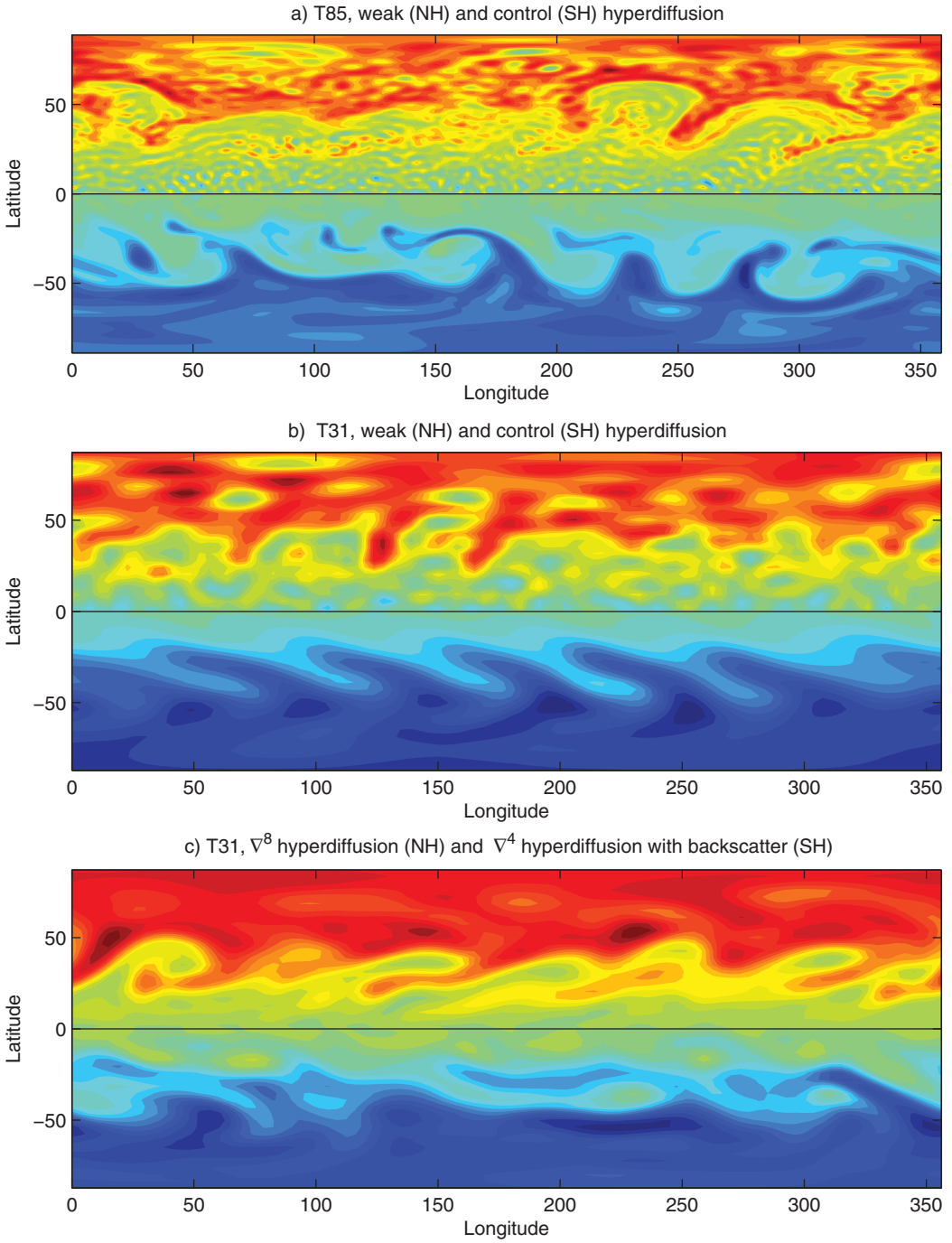

Figure 1. (a) Snapshots of upper-level absolute vorticity for T85 simulations using the control biharmomic hyperdiffusion (0.1 day damping for the shortest wave, SH) or very weak hyperdiffusion (10 day damping for the shortest wave, NH); (b) Same but at T31 resolution; (c) Same but for T31 simulations using biharmonic hyperdiffusion with energy backscatter (SH) or higher order hyperdiffusion (NH).

section]. The top plot combines results from two different global simulations at T85 resolution using biharmonic hyperdiffusion. In the Southern Hemisphere a simulation is shown in which the damping coefficient is chosen to damp the shortest resolved wave with a 0.1 day timescale (the same damping rate used by HS94), while the Northern Hemisphere shows a simulation in which this coefficient has been severely reduced (by a factor of 100). Both simulations show the familiar signature of midlatitude Rossby wave breaking but in the low diffusion simulation this is also accompanied by a vorticity accumulation at the grid scale, as the hyperdiffusion coefficient is too weak to dissipate the enstrophy cascade. Additionally, Figure 2 shows that hyperdiffusion also has an impact on the model's climatology, particularly in the upper

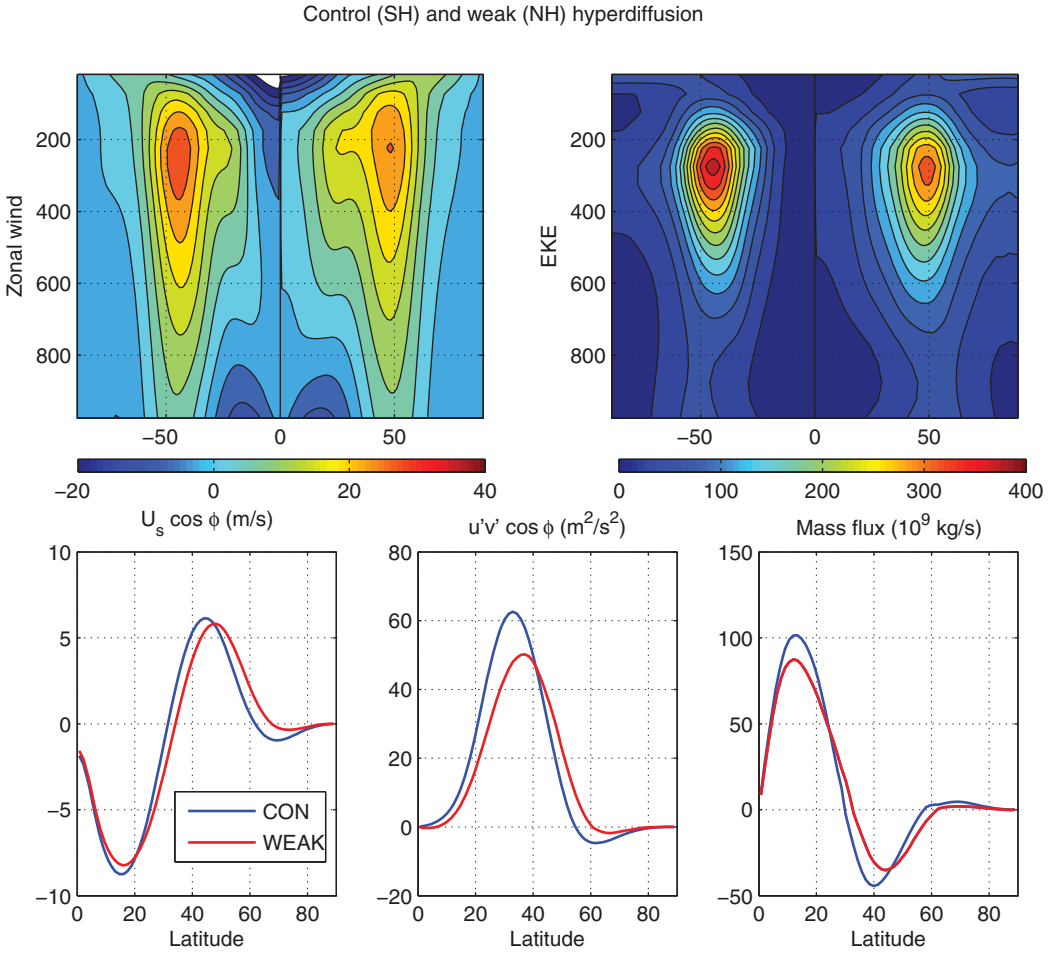

Figure 2. (top) (left) Climatological zonal wind and (right) eddy kinetic energy at T85 using the control hyperdiffusion (SH) or very weak hyperdiffusion (NH). (bottom) Meridional profiles of zonal-mean surface zonal wind, upper-level eddy momentum fluxes and mass streamfunction for the same two simulations.

troposphere. The simulation with the control diffusion (Southern Hemisphere) displays a strong extratropical jet and a sharp midlatitude eddy kinetic energy (EKE) maximum, in good agreement with simulations at higher resolution (c.f., left column of Figure 3). With weak diffusion (Northern Hemisphere) the EKE maximum is smoothed down as there is a leakage of EKE deep into the tropics, and the extratropical jet weakens and moves poleward. Absolute vorticity increases in the subtropical upper troposphere and the Hadley circulation slows down (see Figure 2, bottom). These differences are likely due to changes in the subtropical critical layer, which becomes more nonlinear and less absorbing as hyperdiffusion is reduced [*Killworth and McIntyre*, 1985].

A similar accumulation of grid scale enstrophy and similar circulation biases are found at T31 resolution with low diffusion (see Northern Hemisphere in Figure 1, middle). However, if we use the control hyperdiffusion in this case we obtain a poor climatology, with too weak eddy kinetic energy and eddy fluxes and an overly strong subtropical jet (Figure 3, third column). Likewise, Figure 1 shows that the upper level vorticity has a more wavy structure than in the previous cases, suggestive of quasilinear dynamics. These deficiencies arise as the limited scale separation between the grid and deformation scales makes the latter also sensitive to diffusion.

Thus, choosing the optimal hyperdiffusion coefficient at low resolution requires a trade off between not damping enough grid scale enstrophy and damping too much energy at the deformation scale. The latter implies an artificial damping of the eddies when the inverse cascade is weak and eddies have length scales on the order of the deformation radius [*Schneider and Walker*, 2006]. Even when a significant inverse cascade exists and the energy containing scale itself is not directly affected by diffusion, deformation-scale

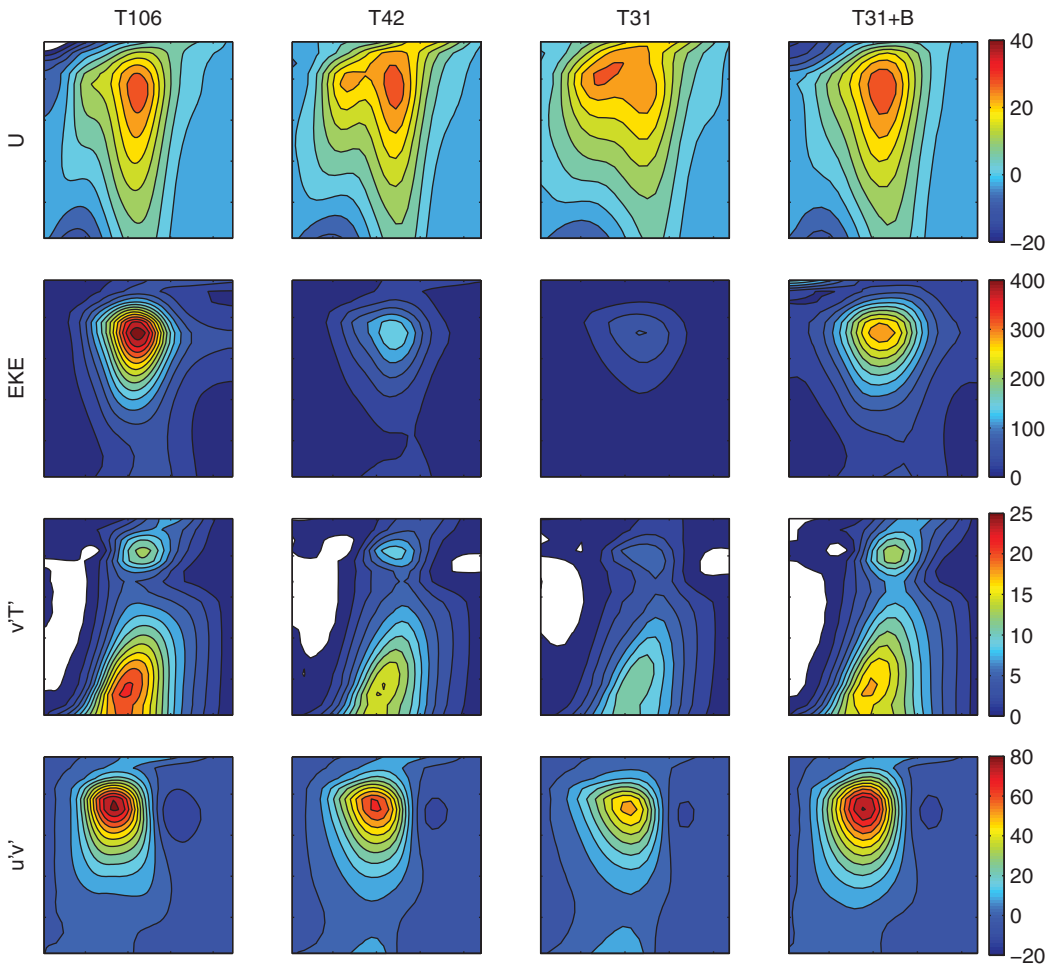

Figure 3. Zonal wind (first row), eddy kinetic energy (second row), eddy heat flux (third row) and eddy momentum flux (fourth row) at T106, T42 and T31 resolutions using the standard hyperdiffusion, and at T31 resolution using kinetic energy-conserving hyperdiffusion.

damping may reduce the large scale energy level by purging some of the energy flux that should feed back into the inverse energy cascade [*Larichev and Held*, 1995]. Hyperdiffusion coefficients are often chosen empirically to produce smoothly decaying eddy kinetic energy spectra with increasing wavenumber near the grid scale, as described by *Boville* [1991] (see also *Jablonowski and Williamson* [2011] for a comprehensive review). For our T31 simulation, it should be clear from the discussion above that the optimal biharmonic diffusion coefficient should lie somewhere between the two values used to produce the snapshots in Figure 1b.

There have been different approaches to deal with this problem, in the turbulence literature [e.g., *Dubos*, 2005; *Hecht et al*., 2008], as recently discussed by *Jansen and Held* [2014], and in the numerical weather prediction (NWP) literature [*Shutts*, 2005; *Berner et al*., 2009; *Tennant et al*., 2011; *Berner et al*., 2012]. The relation between the approach here and in the NWP literature is addressed in the conclusions. [*Jansen and Held*, 2014, JH14 hereafter] have devised a very simple modified subgrid dissipation scheme that can conserve kinetic energy while still dissipating enstrophy as required. In this scheme, the standard ∇^{2n} hyperdiffusion is supplemented with a kinetic energy injection that conceptually accounts for the missing backscatter. At each time step the energy injection rate is determined as a fraction of the hyperdiffusive kinetic energy loss, so that the scheme can be made to exactly conserve kinetic energy if desired. The scheme also dissipates enstrophy provided that the energy injection occurs at larger scales than those at which kinetic energy is dissipated by hyperdiffusion. JH14 test their scheme in idealized quasigeostrophic simulations using two different injection methods that satisfy this constraint, obtaining similar and much improved low-resolution results with both methods. Extending that work, Jansen et al. (submitted, 2015) have derived a variant of the scheme in which the energy injection rate is determined by the local energy budget rather

than global kinetic energy conservation, which is more appropriate for the very inhomogeneous global ocean. Jansen et al. test their scheme in an idealized primitive-equation ocean model, finding again substantial improvement at low resolution.

In this paper we investigate whether the subgrid parameterization proposed by JH14 may also be beneficial for low-resolution atmospheric models. Our motivation is twofold. First, this provides an additional test on the robustness of the scheme, which we implement in a very different model and setting from JH14 and Jansen et al. (submitted manuscript, 2015). It is important to perform a number of such tests to assess the potential benefits of the scheme before it can be implemented in operational ocean models, which still faces many challenges. Additionally, we believe that improving low-resolution atmospheric models has in itself practical value, as discussed above.

We will use as our reference/target simulation the T31 simulation described above, using biharmonic hyperdiffusion and the damping rate of HS94. However, we should stress again that this is *not* the best that one can do using conventional hyperdiffusion. For instance, one can get better results using a more scale-selective diffusion operator (see e.g., the absolute vorticity snapshot using ∇^8 diffusion in the Figure 1, bottom). Even with biharmonic diffusion, better results are obtained using a weaker damping rate as noted above. Our goal is to show that the backscatter parameterization can alleviate the problem of excessive dissipation at low resolution, giving good results in situations in which the conventional formulation would fail to do so. This effectively allows us to choose the hyperdiffusion coefficient without having to worry about its undesired energy damping effects. But we will also show that at even lower resolutions (T21) the best simulation is obtained when a variant of the backscatter parameterization is used.

Our paper is structured as follows. Section 2 describes the model setup and introduces the backscatter parameterization proposed by JH14. Results are presented in section 3 for a number of test cases and we close with a brief discussion in section 4.

2. Model Setup and Formulation

Assessing the resolution convergence of atmospheric models can be ambiguous due to the resolution dependence of physical parameterizations and their interactions with the numerics [see e.g., *Williamson*, 1999]. Motivated by our desire to evaluate the impact of subgrid dissipation on the *dynamics* of low-resolution models, we use for this study a dry primitive-equation model with highly simplified physics, as in the benchmark proposed by HS94 to validate the dynamical cores of atmospheric models. Diabatic heating is modeled using Newtonian relaxation to a "radiative equilibrium" profile that is statically stable and symmetric about the Equator, while simple Rayleigh friction is used over a boundary layer with prescribed depth $\sigma_b = 0.3$. Our basic setup is the same as in HS94, to which the reader is referred for details. Aspects of the resolution sensitivity of this model and its implications for that of comprehensive models have been investigated by *Boer and Denis* [1997], *Pope and Stratton* [2002], *Wan et al*. [2008], *Gerber et al*. [2008], and *Guemas and Codron* [2011], among others.

We use as dynamical core the spectral model developed at the Geophysical Fluid Dynamics Laboratory (available at http://www.gfdl.noaa.gov/fms), in a configuration with 20 equally spaced vertical levels. Because the Held and Suarez benchmark produces weak stratospheric activity (due to the small mean zonal winds in the stratosphere), our model is less sensitive to changes in vertical resolution than more realistic models [but see *Gerber et al*., 2008]. Our focus here is instead on the sensitivity to horizontal resolution (and the associated horizontal dissipation scheme), which we vary from T21 to T106 using a triangular truncation. Diagnostics are constructed using the last 800 days from simulations 1000 days long, at which point the model's climate is well equilibrated. This basic setup is modified in additional test cases as described in the next section.

Subgrid dissipation is added to the momentum equations using Laplacian operators of various orders:

$$\frac{\partial \mathbf{u_h}}{\partial t} = \ldots - \kappa(-1)^n \nabla^{2n} \mathbf{u_h}, \tag{1}$$

where $\mathbf{u_h}$ is the horizontal velocity, ∇^2 is the horizontal Laplacian and n is the hyperdiffusion order. Our reference simulations use biharmonic diffusion ($n = 2$) but we have also tried higher order operators ($n = 4$). When the resolution changes, the diffusion coefficient κ is varied according to the law $\kappa = \kappa_0 (L/L_0)^\gamma$ where L

is the scale of the shortest resolved wave and κ_0 is the hyperdiffusion coefficient with some reference resolution L_0. In operational models the exponent γ is tuned empirically (for instance, $\gamma=3.2$ in CAM with biharmonic hyperdiffusion, see *Lauritzen et al.* [2014, p. 136]). Here we choose for simplicity to keep the damping rate of the shortest resolved wave constant ($\dot{u}_{dif}/u=-(0.1\,\text{days})^{-1}$) as resolution is changed, which is equivalent to taking $\gamma=2n$. This is motivated by geostrophic turbulence theory, which predicts that the eddy turnover timescale is independent of wavenumber when the grid scale lies in the enstrophy cascade range. No subgrid dissipation is included in the thermodynamic equation.

As discussed in the introduction, subgrid dissipation can have a sizable impact on the deformation scale at low resolution, weakening the eddies and degrading the quality of the simulation. JH14 and Jansen et al. (submitted manuscript, 2015) propose to compensate that loss by injecting back into the model part of the kinetic energy dissipated by hyperdiffusion. JH14 try two different injection schemes, one stochastic and one deterministic, obtaining similar results in both cases. We will use their deterministic scheme, implemented adding an additional forcing to the right hand side of equation (1):

$$\frac{\partial \mathbf{u_h}}{\partial t}=\ldots-\kappa(-1)^n\nabla^{2n}\mathbf{u_h}+\nabla\cdot(\nu\nabla\mathbf{u_h}), \tag{2}$$

where ν is a *negative* viscosity, so that the last term injects energy into the model. A similar approach has been used by *Thuburn et al.* [2014] in the context of barotropic turbulence. Note that when energy is conserved this scheme provides a net enstrophy sink as long as $n>1$, in which case energy injection by the negative viscosity forcing occurs at larger scales than the hyperdiffusive dissipation.

Previous studies have used two different approaches to parameterize negative viscosity. JH14 employ a time-dependent but spatially uniform ν, which they calculate under the condition that the energy injection by this term equals a fraction ($r\leq 1$) of the hyperdiffusive energy dissipation at each time step. We will follow the same approach (with $r=1$ for simplicity), except for the fact that we will consider a height-dependent ν and calculate it enforcing kinetic energy conservation independently at each level (it would not be appropriate to inject in the stratosphere some of the kinetic energy dissipated in the troposphere, for instance). We thus calculate $\nu(z,t)$ from the equality:

$$\nu\int\int\left(\nabla^2\mathbf{u_h}\right)\cdot\mathbf{u_h}dA=(-1)^n\kappa\int\int\left(\nabla^{2n}\mathbf{u_h}\right)\cdot\mathbf{u_h}dA \tag{3}$$

This is the scheme that we employ in most of our simulations, except at very low resolution, when usage of a uniform viscosity coefficient produces poor results (for reasons to be discussed later). This deficiency can be corrected using an inhomogeneous viscosity scheme, which we implement following Jansen et al. (submitted manuscript, 2015). The scheme is based on the following local budget for the subgrid eddy kinetic energy e:

$$\frac{\partial e}{\partial t}=H-B-\frac{e}{\tau_f}+K_e\nabla^2 e \tag{4}$$

In this formalism subgrid EKE is created by the hyperdiffusive dissipation H, which absorbs the direct energy flux to small scales, and lost through backscatter B to the resolved scales. There is a frictional damping of e (for which we use the same level-dependent damping timescale $\tau_f(\sigma)$ as for the resolved flow) and also a diffusion of subgrid kinetic energy. The latter allows us to control the extent to which H and B balance locally in equilibrium by changing K_e. Note that this formulation involves an additional computational cost, due not just to the computation of e but also to the increased cost of computing the diffusive term when ν is not constant. Both factors increase the computing time by about a 25% compared to the case with homogeneous viscosity.

From the momentum equations, the local kinetic energy tendencies due to hyperdiffusion and negative viscosity are:

$$\left(\frac{\partial K}{\partial t}\right)_\kappa=-(-1)^n\kappa\left(\nabla^{2n}\mathbf{u_h}\right)\cdot\mathbf{u_h} \tag{5}$$

$$\left(\frac{\partial K}{\partial t}\right)_\nu=[\nabla\cdot(\nu\nabla\mathbf{u_h})]\cdot\mathbf{u_h} \tag{6}$$

where $K=\frac{1}{2}(\mathbf{u_h}\cdot\mathbf{u_h})=\frac{1}{2}(u^2+v^2)$ is kinetic energy. One problem with using these tendencies to force the subgrid kinetic energy equation is that the resulting formulation would not be Galilean invariant. Alternative

formulations that also satisfy global kinetic energy conservation can be derived adding the divergence of a flux to the above tendencies. For instance, if we integrate the $\left(\frac{\partial K}{\partial t}\right)_v$ tendency by parts we obtain:

$$\left(\frac{\partial K}{\partial t}\right)_v = \nabla \cdot (\nu \nabla K) - \nu(|\nabla u|^2 + |\nabla v|^2),$$

Only the second term affects the global kinetic energy budget, as the first term integrates to zero. Additionally, we have found that when the full tendency is used to force the model the upgradient kinetic energy transport by negative viscosity (first term) largely cancels the spatial structure created by the hyperdiffusive forcing, producing too diffused subgrid energy patterns. Results are much improved when the subgrid kinetic energy equation is forced using the second term alone:

$$B = -\nu(|\nabla u|^2 + |\nabla v|^2) \tag{7}$$

For consistency the hyperdiffusive source is also integrated by parts. In our spectral model, this is most easily formulated in terms of vorticity ξ and divergence D:

$$H = -(-1)^n \kappa \left(\xi \nabla^{2(n-1)} \xi + D \nabla^{2(n-1)} D\right) \tag{8}$$

Finally, negative viscosity is computed at all times and positions using the closure:

$$\nu = -V \cdot L \tag{9}$$

where L is a resolution-dependent characteristic length scale and V is estimated using the subgrid energy level: $V = \sqrt{max(e, 0)}$. This expression takes into account that e may occasionally become negative, as noted by Jansen et al. (submitted manuscript, 2015). All dimensionless prefactors are absorbed in the definition of L.

As a final technical point, we note that since $\nu < 0$ the negative viscosity forcing will tend to strengthen velocity gradients. To minimize the impact of this upgradient momentum flux on the mean state we chose to apply the negative viscosity forcing to the eddy component of the flow, after subtracting the zonal mean. When the negative viscosity is applied to the full flow at low resolution, climatological jets are a bit stronger (which may be detrimental or beneficial depending on the nature of the biases for the specific simulation considered) but the results are otherwise very similar.

3. Results

3.1. Control Setting

3.1.1. Resolution Sensitivity

As noted above, a number of previous studies have investigated the resolution sensitivity of Held and Suarez-like models using different dynamical cores and configurations [*Boer and Denis*, 1997; *Pope and Stratton*, 2002; *Wan et al*., 2008; *Guemas and Codron*, 2011, etc.]. A robust feature in all these studies is an increase in eddy strength with resolution, which also impacts eddy fluxes and the strength of the energy cycle. Consistent with the increased eddy heat flux, models also tend to produce extratropical warming as resolution is enhanced, a well-known trend in comprehensive atmospheric models [see *Hack et al*., 2006, and references therein]. Most models (but not all) [see e.g., *Pope and Stratton*, 2002] predict a poleward jet shift with increasing resolution. *Guemas and Codron* [2011] argue that this is due to changes in latitudinal resolution while changes in longitudinal resolution may have the opposite effect, which could make the sensitivity of jet latitude to resolution nonmonotonic. An additional caveat regarding the sensitivity of jet position is that annular variability is very persistent in this model [*Gerber and Vallis*, 2007], so that long integrations may be required for convergence [*Wan et al*., 2008]. Broadly speaking, previous studies have established numerical convergence for the dry dynamical core at resolutions somewhere between T42 and T85 depending on the model and the field considered, with mean fields converging at lower resolution than eddy fluxes.

Figure 4 provides an overview of resolution sensitivity in our model (fields are shown for the Northern Hemisphere only after averaging both hemispheres). Figure 4a shows that surface winds strengthen as resolution is enhanced, and also shift *equatorward* (contrary to most previous studies). To make sure that this is not a sampling artifact, we also show dashed the results from the much longer simulations described in section 3.2. The sensitivity of the jet latitude to resolution is reduced with weaker hyperdiffusion (not shown)

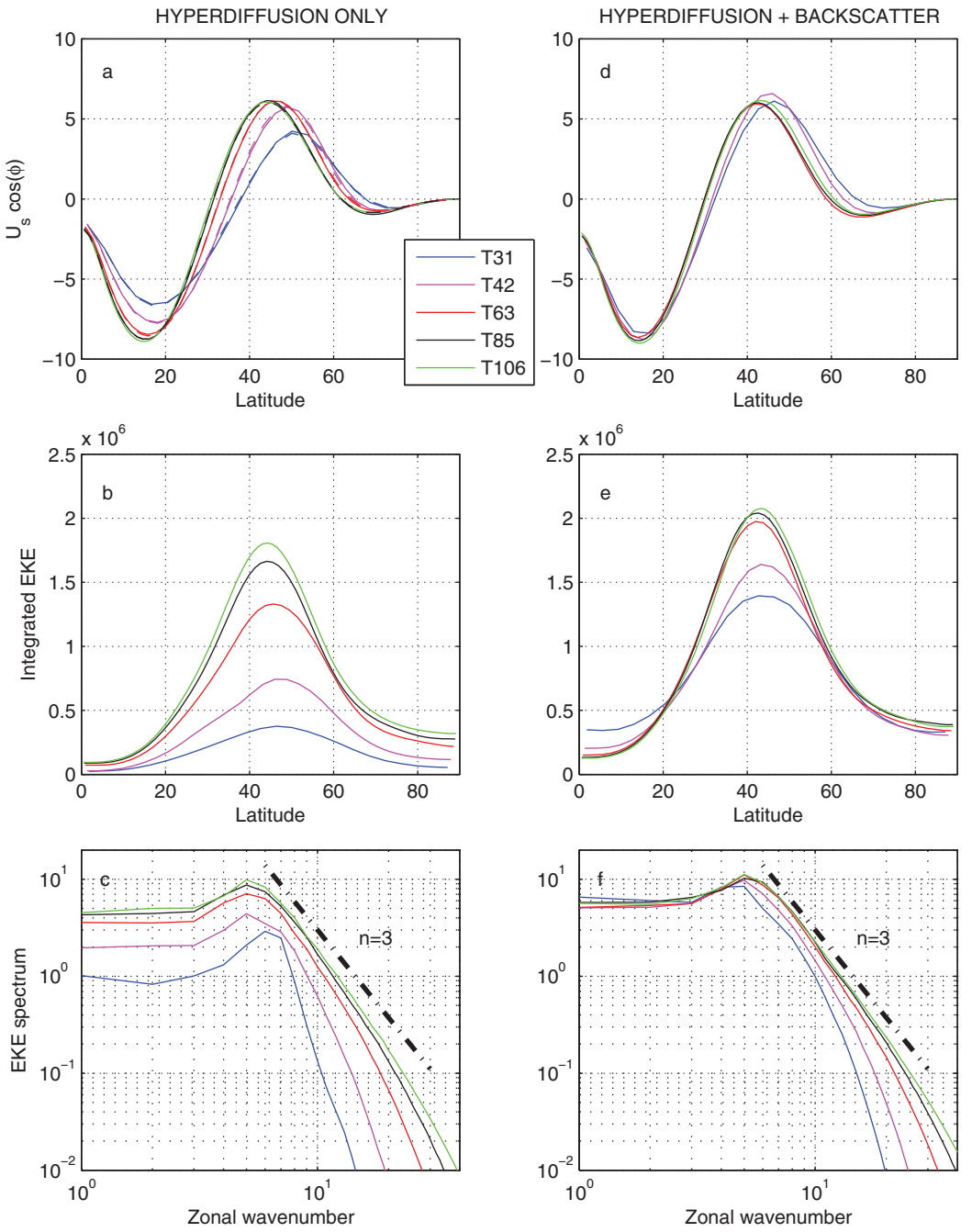

Figure 4. Sensitivity to resolution of (a, d) lowest-level zonal wind (weighted by the cosine of latitude); (b, e) vertically integrated EKE; and (c, f) EKE spectra (30–60° and surface to 100 hPa average). Figures 4a–4c correspond to simulations using standard hyperdiffusion and Figures 4d–4f to simulations also including the energy backscatter scheme. The resolution is indicated with the legend in Figure 4a.

and is also sensitive to vertical resolution [*Gerber et al.*, 2008]. Figure 4b highlights the strong sensitivity of eddy kinetic energy on resolution in these simulations, even for the higher resolutions examined. Interestingly, the spectra in Figure 4c show that this EKE increase is not due to the additional scales included as resolution is enhanced: *energy increases uniformly at all scales*.

We next analyze the impact of the increased eddy energy level on the global entropy budget. As discussed by *Lapeyre and Held* [2003], this is similar to the traditional energy cycle of *Lorenz* [1967] but has the advantage of not requiring the definition of a reference static stability. Figure 5a (solid lines) shows the contributions of all nonconservative processes to the global entropy budget, calculated as heating rates divided by

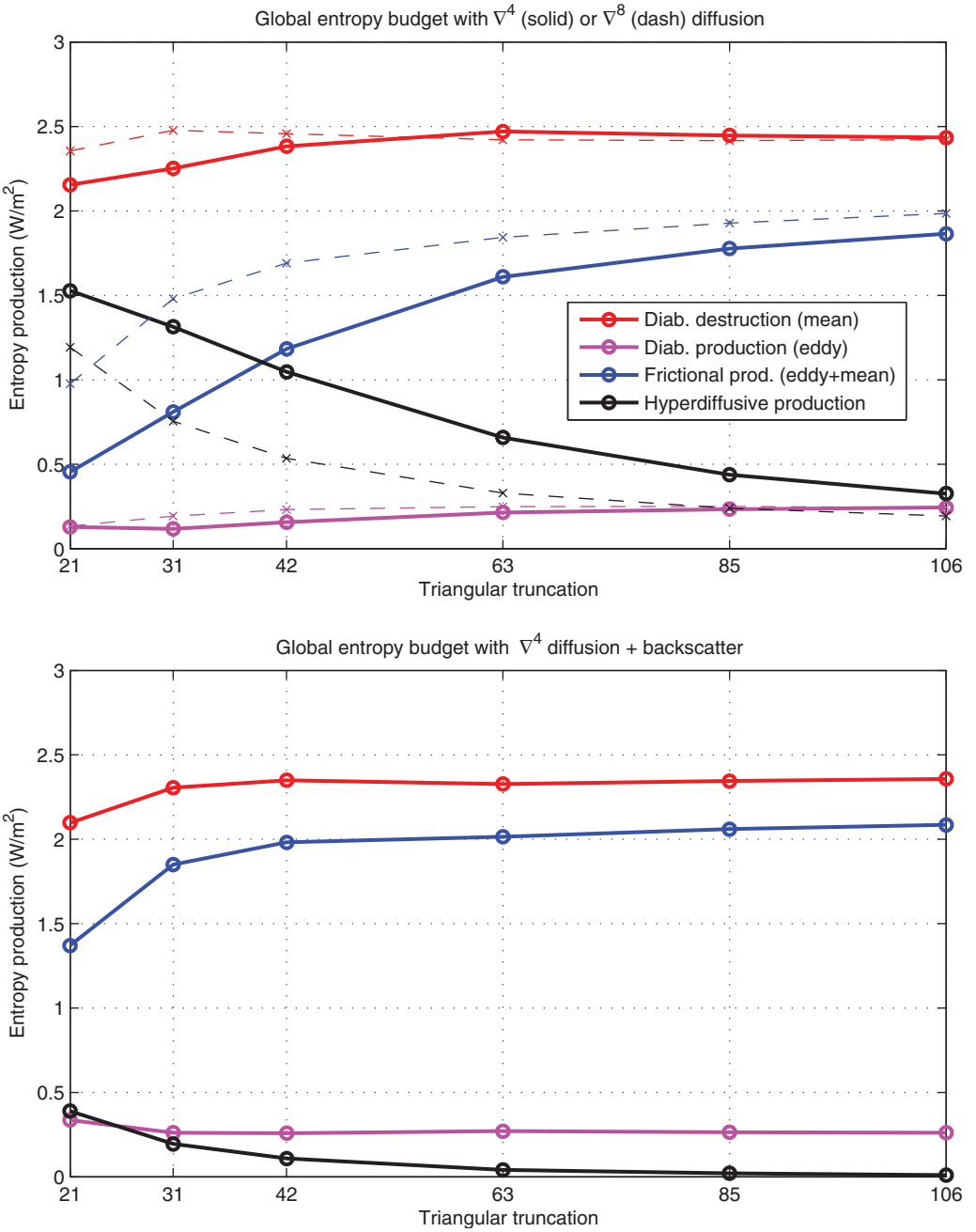

Figure 5. (a) Contributions of zonal-mean diabatic heating (red), eddy diabatic heating (magenta), frictional damping (blue) and hyperdiffusive damping (black) to the global entropy budget, as a function of resolution. Entropy tendencies per unit area are shown multiplied by a reference temperature $T=300$K to give W/m^2 units. The thick, solid lines correspond to simulations using biharmonic hyperdiffusion and the thin, dashed lines to simulations using ∇^8 hyperdiffusion; (b) Same but for simulations using biharmonic diffusion with energy backscatter. The small tendency by hyperdiffusion in this case arises because the subgrid scheme is not exactly kinetic energy conserving when negative viscosity is applied to the eddies only.

temperature (for more details, see e.g., *Peixoto and Oort* [1992]). At high resolution the main entropy source is frictional dissipation, with a much smaller contribution by the diabatic eddy damping and the hyperdiffusion scheme. This entropy production is balanced by the diabatic destruction of entropy by the zonal-mean heating. However, as resolution is degraded the hyperdiffusive source increases at the expense of the frictional production, becoming the dominant entropy source at resolutions coarser than T42. The resolution sensitivity of frictional entropy production mirrors that of global eddy kinetic energy, which is not yet fully converged even at resolutions as high as T85 (Figure 6a).

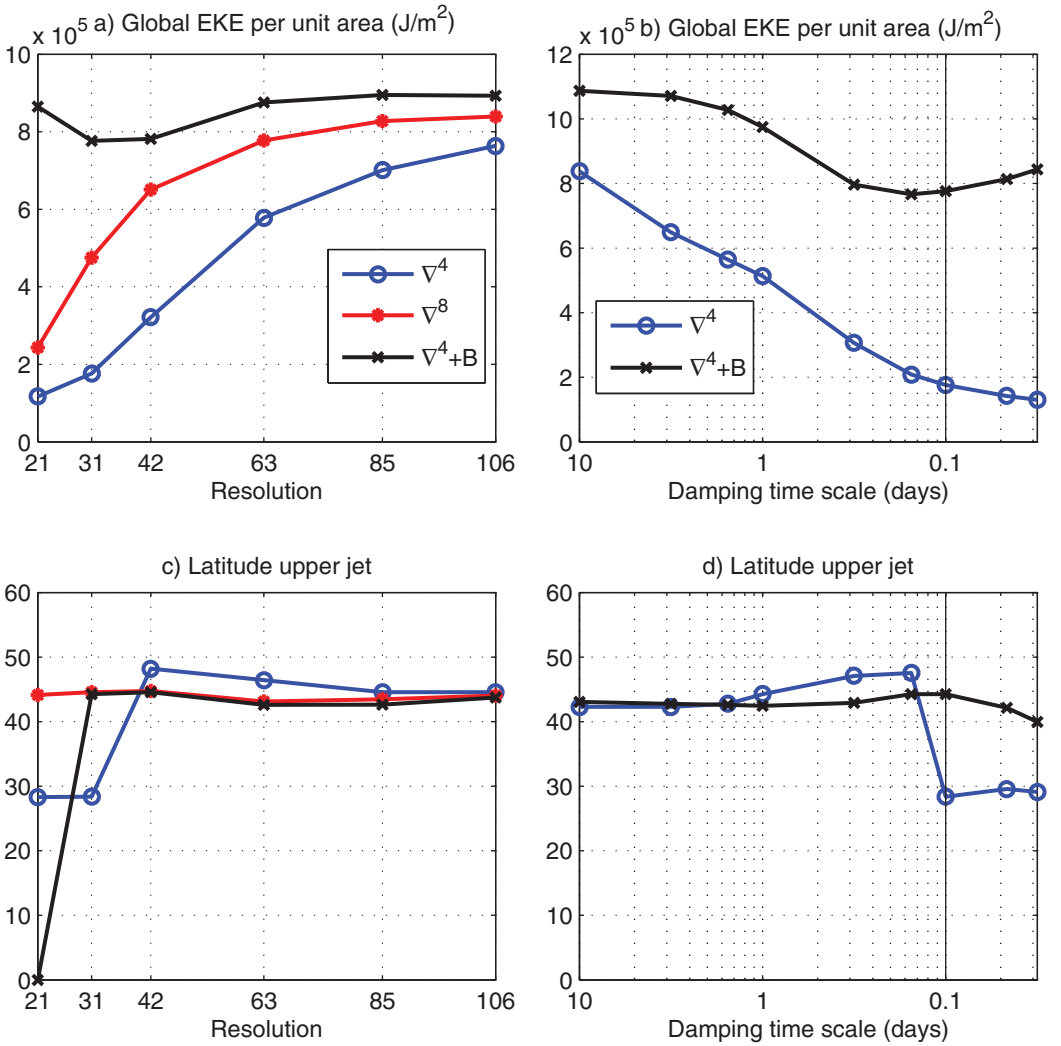

Figure 6. Resolution sensitivity of (a) globally integrated eddy kinetic energy and (c) latitude of upper level wind maximum for simulations using biharmonic diffusion (blue), ∇^8 diffusion (red) or biharmonic diffusion with energy backscatter (black). (b, d) Same but as a function of hyperdiffusion at T31 resolution. The vertical lines indicate the control diffusion.

In contrast with the strong sensitivity of the model's EKE and frictional entropy production on resolution, the strength of the global entropy cycle (as measured by the diabatic destruction term) appears to converge somewhere between T42 and T63. This occurs as eddy fluxes are much less sensitive to resolution than eddy energies (Figure 3), for reasons we do not fully understand. At T63 the eddy fluxes are very similar to the converged T106 fluxes (not shown), while at T42 they are only a bit weaker. These eddy flux biases are responsible for biases in the model's climatology: the weak eddy heat flux leads to too strong vertical shears and subtropical jet, while the weak eddy momentum flux produces too weak surface westerlies. The biases become much more severe as the eddy fluxes further weaken at T31 and T21 resolutions –for those simulations, the upper level wind maximum moves to the subtropics (Figure 6c).

One can reduce the damping effect of the hyperdiffusion scheme by employing a more scale-selective operator. Results using ∇^8 diffusion are also included in Figures 5 and 6 for comparison. Although frictional entropy production (Figure 5a) and global EKE (Figure 6a) are less sensitive to resolution at high resolution, there is still a significant sensitivity for resolutions coarser than T63. However this reduction in EKE again appears to have a limited impact on the eddy fluxes, so that the mean state is robust down to the coarsest resolution (Figure 6c). With both forms of diffusion the mean state only starts degrading at resolutions at which hyperdiffusion becomes the dominant entropy source, which occurs at T42 with biharmonic hyperdiffusion and at T21 with ∇^8 diffusion.

3.1.2. Homogeneous Negative Viscosity

As Figure 4c shows, grid scale dissipation does not only damp the grid scale but it also reduces the energy level at larger scales. Even when the energy-containing eddies are not directly affected by diffusion, hyperdiffusive dissipation may impact kinetic energy levels by purging some of the upscale energy flux. Since this is the motivation for the energy backscatter parameterization of JH14, it is intriguing whether that parameterization may also improve our low resolution simulations.

Figures 4d and 4e show robust low-resolution improvements in surface winds and eddy kinetic energy and enhanced numerical convergence with (homogeneous) negative viscosity. Most strikingly, all simulations now exhibit realistic large scale EKE spectra, with comparable energy levels and a well-defined $n = 3$ slope in the inertial range (Figure 4f). The T31 simulation is described in more detail in the last column of Figure 3. Compared with the previous simulation using the standard scheme (third column), eddy heat and momentum fluxes are much improved and biases in the zonal wind climatology nearly eliminated. Additionally, upper level snapshots of absolute vorticity now have a realistic structure (Figure 1c, Southern Hemisphere). The main deficiencies of this simulation, which might be related, are a slight poleward bias in the surface westerlies and an excessively diffuse EKE pattern. The latter is likely due to our use of a constant viscosity that spreads the kinetic energy injection horizontally into the tropics.

The sensitivity of the global entropy cycle and mean state on resolution with the backscatter scheme is also described in Figures 5 and 6. The scheme clearly improves the global eddy kinetic energy and associated frictional entropy production term at all resolutions. It also produces a good climatology at resolutions T31 and higher (but so did the original scheme for resolutions higher than T42, in spite of the weak EKE). On the other hand, the homogeneous-viscosity T21 simulation is deficient, displaying too weak surface westerlies and an Equatorial westerly maximum (see third column of Figure 7). We discuss this simulation in more detail in the next subsection.

As noted in the introduction, one advantage of the kinetic energy-conserving hyperdiffusion scheme is that it allows us to change the strength of subgrid dissipation without having to worry about its damping effects on the eddies. This is illustrated in Figures 6b and 6d, which describe the sensitivity of the model's climatology on large changes in the diffusive damping rate for T31 simulations using the standard hyperdiffusion and kinetic energy-conserving hyperdiffusion. The sensitivity is weaker with the latter, most notably in terms of the model's EKE. The kinetic energy-conserving scheme also prevents the weakening of the westerlies and the transition to a subtropical jet regime that occurs with the conventional scheme when diffusion is sufficiently high.

3.1.3. The T21 Simulation

As the results of the previous subsection show, use of the backscatter parameterization improves the simulations at resolutions T31 and higher but at T21 results are actually worse with this parameterization than with the standard formulation. In contrast, one can get reasonable results at this resolution if ∇^8 instead of biharmonic diffusion is used. The first three columns of Figure 7 show the mean state and eddy fluxes at T21 resolution for simulations using standard biharmonic diffusion, ∇^8 diffusion and biharmonic diffusion with homogeneous negative viscosity, respectively. These can be compared with the converged T106 simulation in the first column of Figure 3 (note that the same color scale is used in both figures). With standard biharmonic diffusion the eddy kinetic energy and fluxes are very weak, so the extratropical jet is also weak and the upper level wind maximum is found in the subtropics. Results improve with ∇^8 diffusion, which does not damp the eddies as much. Eddy kinetic energy is still much weaker than in the T106 simulation but because the eddy heat and momentum fluxes are not reduced as much this simulation has a reasonable climatology. The extratropical jet is a bit too weak (and too far poleward) and the subtropical jet is a bit too strong, but biases are much smaller than with biharmonic diffusion.

In both previous cases, simulation biases were caused by too weak eddy activity. In contrast, biases in the simulation with energy backscatter have a different flavor. It is not so much the strength of the eddies that is wrong, but their spatial distribution. Although the midlatitude EKE maximum is significantly weaker than at T106 resolution, both simulations have in fact very similar eddy kinetic energy in the global mean (c.f., Figure 6a). The difference in midlatitude EKE between both simulations results from the very diffused EKE pattern in the backscatter simulation. Albeit to a lesser extent, the same was found at T31 resolution as discussed above (c.f., Figures 3 and 4e). This suggests that the backscatter parameterization is doing a

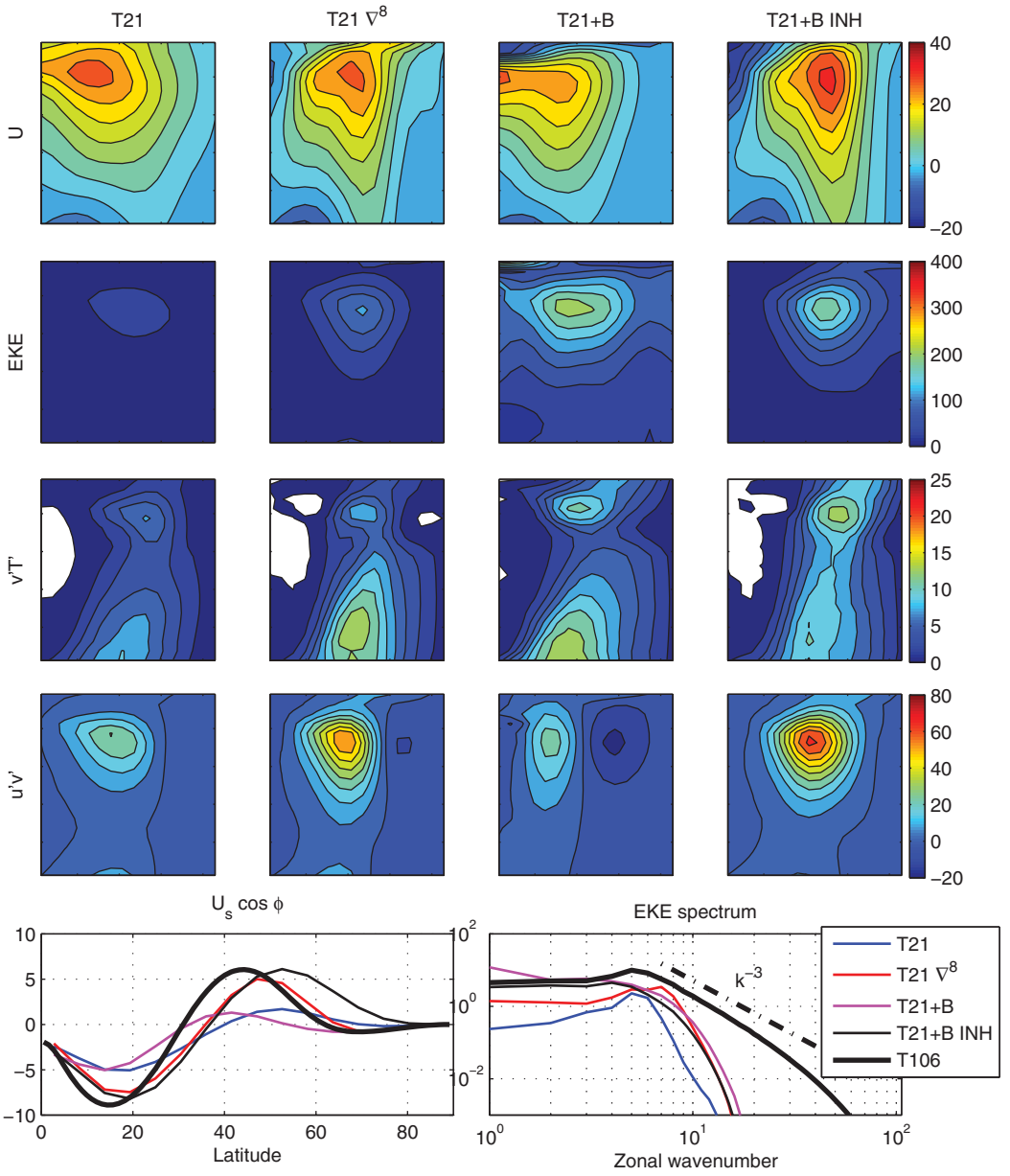

Figure 7. As Figure 4 but for simulations at T21 resolution using biharmonic diffusion (first column), ∇^8 diffusion (second column), and biharmonic diffusion with energy backscatter with horizontally uniform (third column) or inhomogeneous (fourth column) viscosity. The bottom two figures show surface zonal wind profiles and eddy kinetic energy spectra for the same simulations and for the converged T106 simulation.

reasonable job injecting back the kinetic energy dissipated by the hyperdiffusive scheme but failing in terms of the injection location.

To test this hypothesis, we compare in Figures 8a, b the spatial patterns of kinetic energy injection by negative viscosity in the T31 and T21 simulations with the spatial pattern of hyperdiffusive dissipation in the T63 simulation, rescaled to have the same global mean dissipation as the above simulations. (We do not show the actual dissipation patterns for the T21 and T31 simulations because we have found that these patterns are affected by biases in the spatial structure of the eddies arising from biases in kinetic energy injection). In the turbulent situation that we are hoping to parameterize, the energy backscatter should occur at roughly the same spatial locations at which kinetic energy is fluxed to the small scales. The hyperdiffusive kinetic energy dissipation pattern (blue line) exhibits a strong midlatitude maximum, a bump in the subtropics and

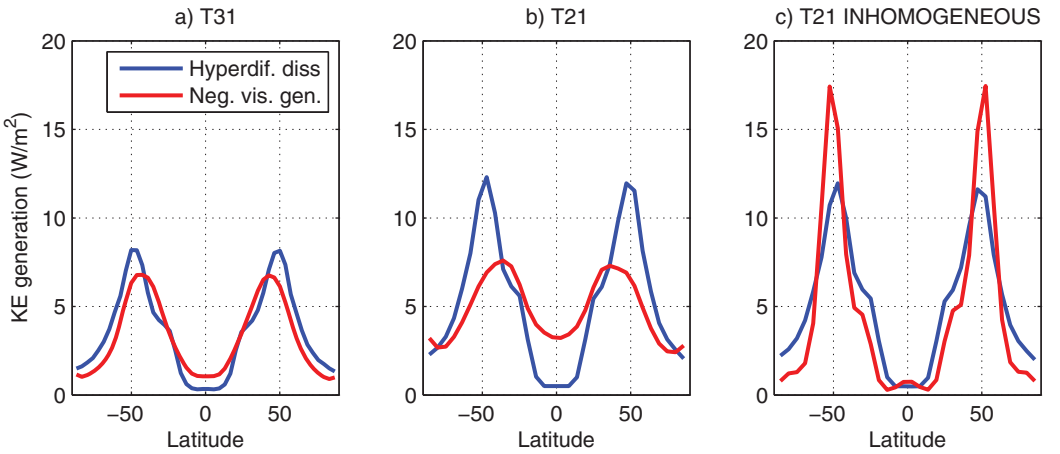

Figure 8. Vertically integrated hyperdiffusive kinetic energy loss (blue) and negative viscosity kinetic energy generation (red) as a function of latitude for (a) T31 backscatter simulation, (b) T21 backscatter simulation, and (c) T21 backscatter simulation with inhomogeneous negative viscosity. The hyperdiffusive dissipation for all figures (blue lines) was actually computed rescaling the dissipation pattern in the T63 simulation to have the same global integral as the specified simulation, for reasons discussed in the text.

very small values in the tropics. At T31 resolution, the negative viscosity kinetic energy generation is shifted equatorward of the dissipation, but biases are small. In contrast, the T21 pattern is clearly deficient, with too weak midlatitude injection and too strong injection in the tropics, which likely accounts for the diffused EKE structure in this simulation. These injection biases have an impact on the mean state: we suspect that the upper troposphere westerly maximum at the Equator in this simulation might be driven as Rossby waves forced by the negative viscosity scheme at low latitudes propagate out of the region (the generation of Equatorial eddies is one of the best known mechanisms leading to superrotation, see e.g., *Kraucunas and Hartmann* [2005]).

Aiming to correct this injection bias, we have repeated the T21 simulation using the inhomogeneous viscosity scheme of Jansen et al. (submitted manuscript, 2015). As described in section 2 negative viscosity scales with the *local* subgrid kinetic energy in this scheme, so that the energy backscatter is more constrained by the dissipation pattern than in the homogeneous viscosity case. The scheme requires two parameters: the characteristic length scale L and the subgrid kinetic energy diffusivity K_e. For all simulations in this paper we have taken $L=150$ km and $K_e=1.16\times10^6$ m^{2}s^{-1} but results are very robust to changes in these parameters and/or in friction (as also found by Jansen et al. (submitted manuscript, 2015)). Although L has a strong impact on the subgrid kinetic energy level, the backscatter and the resolved climate are much less sensitive to changes in this parameter.

Figure 8c shows the pattern of backscatter energy injection for the T21 simulation with the inhomogeneous viscosity scheme. Despite the significant biases (the injection is a lot more peaked than the dissipation and its maximum too far poleward), the Equatorial injection is strongly reduced with the new scheme, which seems crucial for obtaining a good climate. Figure 7 (last column) shows that the eddy kinetic energy is now nicely contained in the extratropics and superrotation is no longer found. Although this simulation is not fully satisfying (the extratropical jet is too strong and poleward shifted), these results provide nonetheless a significant improvement compared to simulations using conventional hyperdiffusion or homogeneous viscosity backscatter.

3.2. Internal Variability

Getting the right eddy kinetic energy level should also be important for the internal variability. As an additional test on the benefits of the backscatter scheme we have studied its impact on the annular variability of the Held and Suarez model, which is known to be sensitive to resolution [*Gerber et al*., 2008]. We define the zonal index as the principal component of the leading mode of variability of the zonal-mean zonal wind, integrated between the surface and 225 hPa, over the latitudinal range 10–80. Figure 9a shows the structure of this mode at T85 resolution, expressed as the regression of the full $\bar{U}(y,p)$ on the standarized principal component time series. This mode is associated with a meridional shift of the extratropical jet about its mean position. Although the structure of the mode is robust as resolution changes, the amplitude

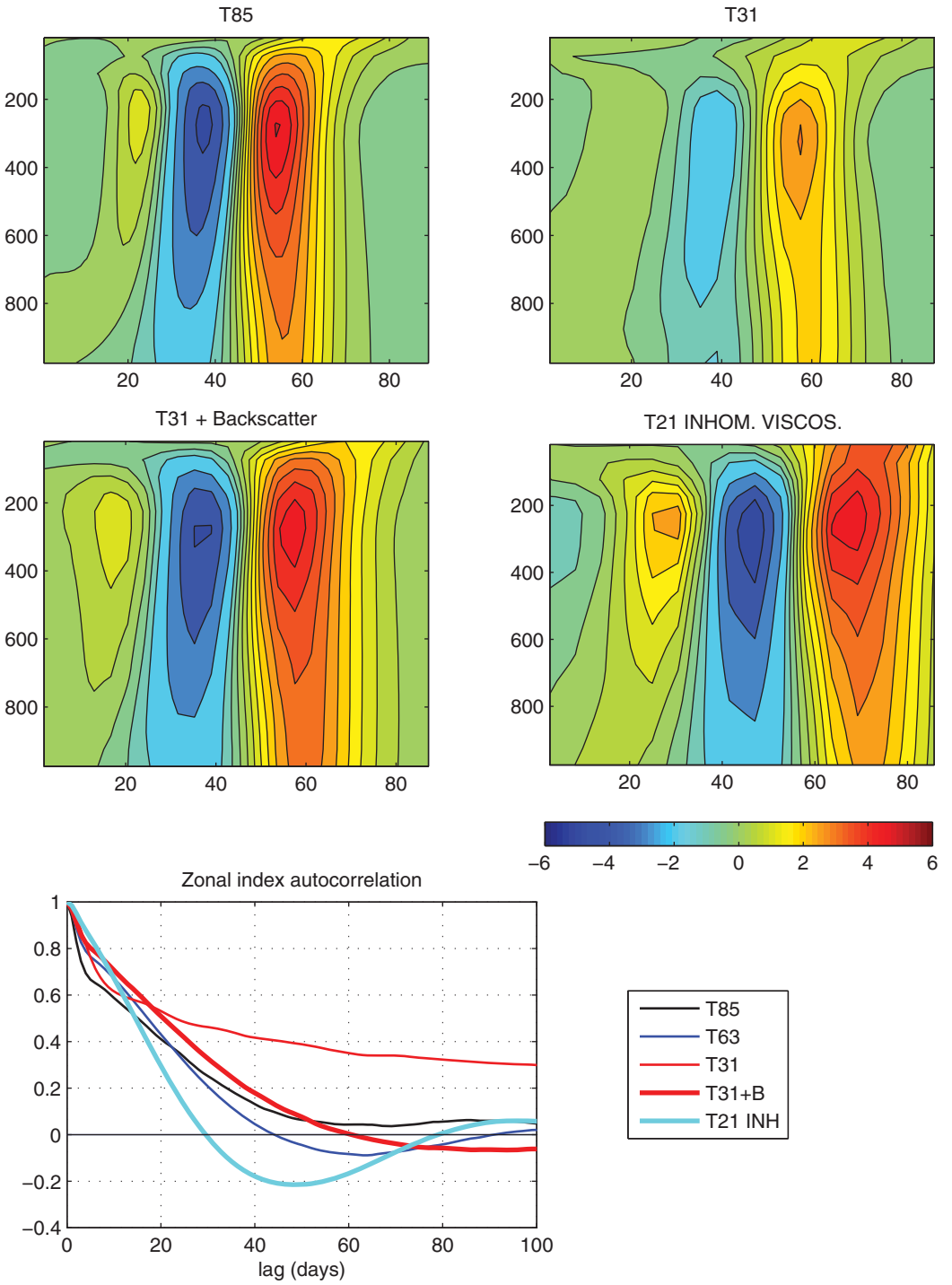

Figure 9. Regression of zonal-mean zonal wind on the standarized leading mode of zonal wind variability at (a) T85 and (b) T31 resolutions using the standard hyperdiffusion, (c) T31 resolution with homogeneous viscosity backscatter, and (d) T21 with inhomogeneous viscosity (e) Autocorrelation of the associated principal components for the same simulations.

of this variability weakens with coarsening resolution. For instance, the zonal-wind regression roughly halves at T31 resolution (Figure 9b).

Lorenz and Hartmann [2001] show that eddy memory makes annular mode variability more persistent than for the prototype first order autoregressive process damped by friction. The enhanced memory is provided by the sensitivity of the eddy fluxes on the anomalous mean state, though the dynamical mechanism

involved is still debated [*Lorenz*, 2014; *Zurita-Gotor et al*., 2014]. Thus, biases in the decorrelation timescale of the annular mode may indicate a poor representation of the eddy processes and/or their interaction with the mean flow. Figure 7e compares the autocorrelation function of the zonal index time series for simulations at various resolutions, computed using extended (24,000 days long) integrations. The e-folding timescale for a converged simulation is order 30 days, significantly more persistent than in the atmosphere [*Gerber et al*., 2008].

The e-folding timescale more than doubles for the T31 simulation, which exhibits extremely long persistence. This is an important concern because the correct representation of eddy feedbacks in a model is also crucial for its sensitivity to external forcing [*Ring and Plumb*, 2008; *Lutsko et al*., 2015]. As mechanisms of climate variability on millennial timescales often need to be tested using low-resolution models, it is important that these models have a realistic annular variability. Results are much improved when kinetic energy-conserving hyperdiffusion is used. The T31 simulation with homogeneous negative viscosity has an annular mode with the correct amplitude (Figure 9c) and persistence (Figure 9e, thick blue line). Even at T21 one can get reasonable results using the inhomogeneous viscosity scheme (Figure 9d), though the annular mode is shifted poleward (consistent with the climatological jet bias for this simulation) and the autocorrelation function displays more of an oscillatory behavior.

3.3. Asymmetric Climates

In the simulations presented above, reasonable results were obtained using the simple homogeneous viscosity scheme at resolutions T31 and higher. However, the idealized HS94 benchmark is also very homogeneous, displaying hemispheric and zonal symmetry. To investigate whether the homogeneous viscosity scheme also works well in less idealized settings we have investigated the resolution sensitivity of a longitudinally dependent climate with a midlatitude stormtrack. This is achieved by adding to the radiative equilibrium profile a localized heating term using the analytical expression proposed by *Gerber and Vallis* [2007] with a maximum heating rate $A=4\,\mathrm{K/d}$. Asymmetric heating is applied in the Northern Hemisphere only. Simulations are run for 3500 days now and diagnostics computed using the last 3000 days.

Figure 10 shows the lower level temperature (contours) and upper level EKE (shading) for this benchmark at various resolutions. We observe a baroclinic zone near the central longitude, with the stormtrack peaking slightly downstream. Although this basic structure is well reproduced at resolutions T42 and higher, the amplitude of the eddies is sensitive to resolution and the stormtrack is too weak even at T63 resolution. At T31 resolution the stormtrack structure is also wrong, displaying two independent eddy amplitude maxima instead of a single one. This simulations is much improved with the homogeneous viscosity scheme (Figure 10d), which boosts the amplitude of the eddies and produces better results than the T63 simulation. As the main bias, this simulation exhibits too strong longitudinal localization, with a stormtrack that is too broad at the maximum and too weak in the far field. Finally, Figure 10e shows the T21 results using the inhomogeneous viscosity scheme. Although the stormtrack has a reasonable structure, the eddies are a bit too weak.

4. Discussion

The simulations presented in this paper strengthen the case made by *Jansen and Held* [2014] on the benefits of energetically consistent subgrid dissipation schemes for atmospheric and oceanic simulations. Robust improvements are found in our model when conventional hyperdiffusion is replaced with a kinetic energy-conserving subgrid scheme in idealized case studies. Although the impact of the kinetic energy-conserving scheme is most obvious at low resolution, improved results are also found at resolutions as high as T63 (Figure 4). Besides accelerating horizontal resolution convergence (with fixed vertical resolution), an added benefit of the backscatter scheme is that it reduces the sensitivity of the results on the strength of subgrid dissipation.

The kinetic energy-conserving scheme can correct biases in the eddy kinetic energy level found with conventional hyperdiffusion over a wide range of resolutions. However, the impact of the scheme on the model's climatology is more subtle than in the studies of JH14 and Jansen et al. (submitted manuscript, 2015) because the time-mean flow is already nearly converged at T42 resolution using conventional hyperdiffusion in spite of the weak kinetic energy level. Biases in the eddy kinetic energy level only impact the

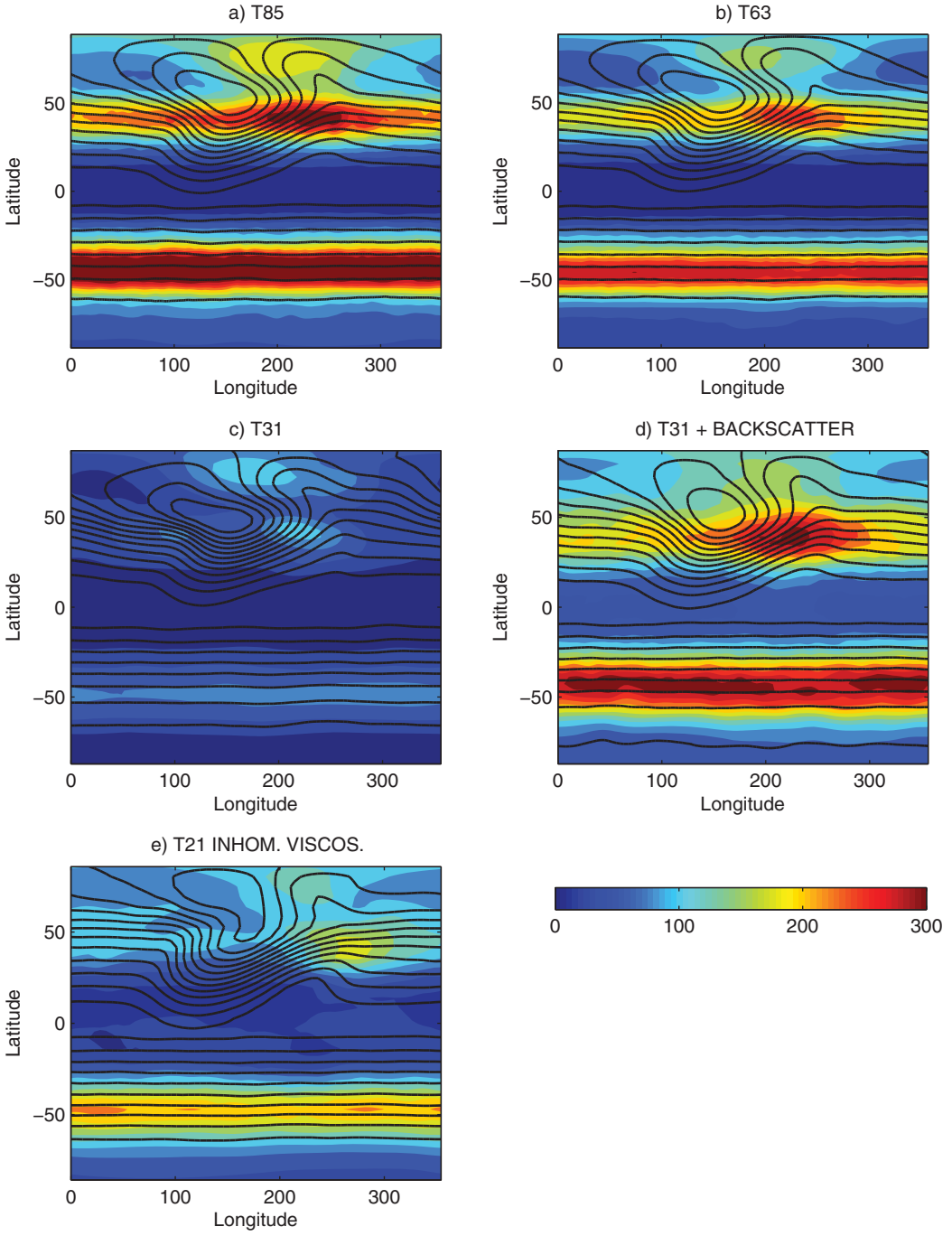

Figure 10. Lowest level temperature (contours) and upper-troposphere eddy kinetic energy (shading) for the stormtrack benchmark described in the text. The horizontal resolution and dissipation scheme for each simulation are indicated in figure titles.

time-mean flow in our model at resolutions T31 and coarser; in those cases, improvements in the eddy kinetic energy level using the backscatter scheme also have a positive impact on the model's climatology.

It is puzzling that the large eddy kinetic energy changes as resolution is varied have so little impact on the strength of the eddy fluxes and on the model's climatology. A striking illustration of this is provided by Figure 11, which shows that the eddy heat and momentum flux cospectra are quite robust as resolution is changed in spite of the large changes found in the eddy kinetic energy spectra (c.f., Figure 4c). Although not emphasized, previous studies have found hints of the same behavior. For instance, reservoirs of eddy kinetic and available potential energy display stronger sensitivity to resolution than barotropic and

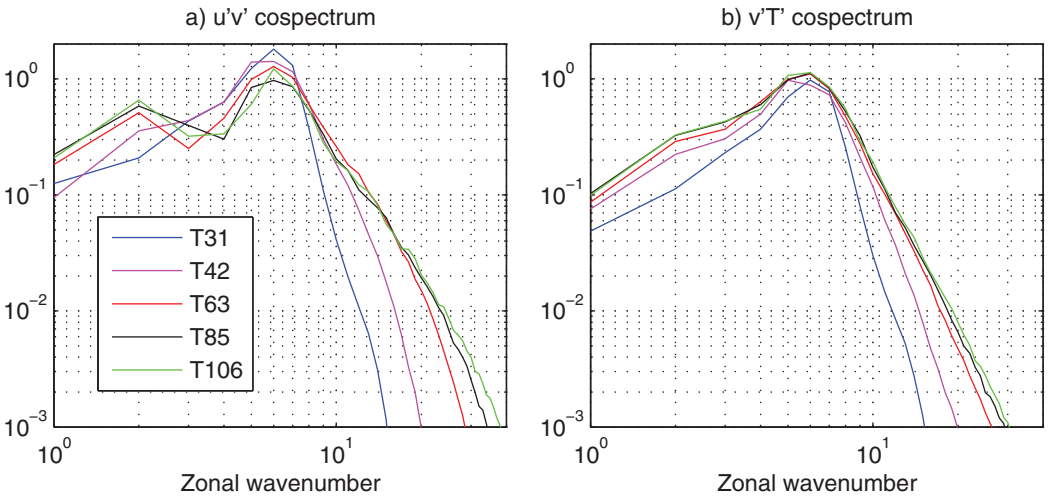

Figure 11. Zonal cospectra (30–60° and surface to 100 hPa averages) of (a) eddy momentum flux and (b) eddy heat flux, as a function of resolution using standard hyperdiffusion.

baroclinic conversions and the strength of the energy cycle in *Pope and Stratton* [2002, Figure 4]. Likewise, *Boer and Denis* [1997] note that changes in eddy correlations (or "eddy efficiencies," in their wording) tend to compensate biases in eddy amplitudes as resolution changes, for both momentum and temperature. This is an intriguing result that casts some doubt on the relevance of closures based on mixing length ideas, at least in this context of sensitivity to horizontal resolution. This behavior, and the more modest success of the kinetic energy-conserving scheme in our simulations compared to those of JH14, is likely due to differences in the setting (atmospheric versus oceanic, see *Jansen and Ferrari* [2012]) rather than to differences in the model.

It has long been known that atmospheric models are too dissipative, particularly when horizontal diffusion operators with limited scale selectivity are used [*MacVean*, 1983]. The notion that energy injection may alleviate this problem is also not new [*Frederiksen and Davies*, 1997; *Shutts*, 2005] and a number of recent studies have shown that stochastic energy backscatter has the potential to improve numerical weather prediction (NWP) models [*Berner et al*., 2009; *Tennant et al*., 2011; *Berner et al*., 2012, and others]. However, there are important differences in scope between those high-resolution studies and the present work. Here, the backscatter is only meant as a complement/improvement to traditional hyperdiffusion, introduced to compensate the excessive dissipation by this scheme (or the implicit diffusion in other schemes) at low/moderate resolutions, when this dissipation may be significant. In this spirit, ratios of energy injection to dissipation (backscatter ratios) close to one are reasonable based on the geostrophic turbulence phenomenology. In contrast, the stochastic backscatter developed for NWP models aims to compensate excessive energy dissipation in models arising not just from hyperdiffusion but also due to other processes like convection or orographic drag. The connection between energy loss and backscatter is more obscure in this case, even for the diffusive component (nonbalanced motions may provide a significant route to dissipation as they become more important at high resolution). In this context, the backscatter ratio becomes a tunable parameter, and values much smaller than one have been typically employed [see e.g., *Sanchez et al*., 2014]. Finally, there are differences in the injection method. Although most previous studies in the NWP literature have used stochastic injection, *Shutts* [2013] argues that this method may not adequately capture the spectral energy injection patterns in the large scale and advocates using deterministic backscatter instead. Along these lines, *Sanchez et al*. [2013] has shown that deterministic energy injection using the vorticity confinement method [*Steinhoff and Underhill*, 1994] can alleviate circulation biases at low resolution due to excessive dissipation/low eddy kinetic energy, consistent with the results presented here.

While our results suggest that getting the eddy kinetic energy right may not be crucial for obtaining realistic mean states in low resolution models, it is still important to do so from a practical perspective because the kinetic energy level is likely to impact other important aspects of a model's climatology related to higher moments and extremes, especially in more realistic models with latent heat release. The weak EKE bias may

also affect the internal variability of low-resolution models and their sensitivity to external forcing, as discussed in section 3.2. Finally, it is important to note that the highly simplified boundary layer scheme used here makes the mean circulation in our model less sensitive to eddy kinetic energy changes than it would be in a model with more realistic physics, in which the heat, momentum and moisture fluxes at the surface would increase with eddy kinetic energy. After showing the feasibility and robustness of kinetic energy-conserving hyperdiffusion for idealized primitive-equation dry models in this paper, it is of interest to assess the benefits of the scheme in more realistic models and settings.

Acknowledgments

P.Z.G is funded by grant CGL2012-30641 by the Ministry of Economy and Research of Spain. The results presented in this work were obtained using the spectral dynamical core available at http://www.gfdl.noaa.gov/fms and the kinetic energy-conserving subgrid scheme described in the manuscript. The output data for all simulations in the paper are stored in the Geophysical Fluid Dynamics Laboratory archive system and can be obtained from the first author (pzurita@alum.mit.edu) upon request. We are grateful to Ed Gerber and an anonymous reviewer for their thorough reviews and pertinent suggestions.

References

Berner, J., G. Shutts, M. Leutbecher, and T. Palmer (2009), A spectral stochastic kinetic energy backscatter scheme and its impact on flow-dependent predictability in the ecmwf ensemble prediction system, *J. Atmos. Sci.*, *66*(3), 603–626.

Berner, J., T. Jung, and T. Palmer (2012), Systematic model error: The impact of increased horizontal resolution versus improved stochastic and deterministic parameterizations, *J. Clim.*, *25*(14), 4946–4962.

Boer, G., and B. Denis (1997), Numerical convergence of the dynamics of a GCM, *Clim. Dyn.*, *13*, 359–374.

Boville, B. A. (1991), Sensitivity of simulated climate to resolution, *J. Clim.*, *4*, 469–485.

Charney, J. G. (1971), Geostrophic turbulence, *J. Atmos. Sci.*, *28*, 1087–1094.

Delworth, T. L., et al. (2012), Simulated climate and climate change in the GFDL CM2.5 high-resolution coupled climate model, *J. Clim.*, *25*, 2755–2781.

Dubos, T. (2005), Frame invariance and conservation in two-dimensional subgrid models, *Physica D*, *202*(1), 1–15.

Frederiksen, J. S., and A. G. Davies (1997), Eddy viscosity and stochastic backscatter parameterizations on the sphere for atmospheric circulation models, *J. Atmos. Sci.*, *54*(20), 2475–2492.

Gerber, E., and G. Vallis (2007), Eddy-zonal flow interactions and the persistence of the zonal index, *J. Atmos. Sci.*, *64*, 3296–3311.

Gerber, E. P., S. Voronin, and L. M. Polvani (2008), Testing the annular mode autocorrelation timescale in simple atmospheric general circulation models, *Mon. Weather Rev.*, *136*, 1523–1536, doi:10.1175/2007MWR2211.1.

Guemas, V., and F. Codron (2011), Differing impacts of resolution changes in latitude and longitude on the midlatitudes in the LMDZ atmospheric GCM, *J. Clim.*, *24*, 5831–5849.

Hack, J., J. M. Caron, G. Danabasoglu, K. W. Oleson, C. Bitz, and J. E. Truesdale (2006), CCSMCAM3 climate simulation sensitivity to changes in horizontal resolution, *J. Clim.*, *19*, 2267–2289.

Hallberg, R. (2013), Using a resolution function to regulate parameterizations of oceanic mesoscale eddy effects, *Ocean Modell.*, *72*, 92–103.

Hecht, M., D. Holm, M. Petersen, and B. Wingate (2008), The lans-α and leray turbulence parameterizations in primitive equation ocean modeling, *J. Phys. A Math. Theor.*, *41*(34), 344009.

Held, I. M., and P. J. Phillips (1987), Linear and nonlinear barotropic decay on the sphere, *J. Atmos. Sci.*, *44*, 200–207.

Held, I. M., and M. J. Suarez (1994), A proposal for the intercomparison of the dynamical cores of atmospheric general-circulation models, *Bull. Am. Meteorol. Soc.*, *75*, 1825–1830.

Jablonowski, C., and D. L. Williamson (2011), The pros and cons of diffusion, filters and fixers in atmospheric general circulation models, in *Numerical Techniques for Global Atmospheric Models*, edited by P. H. Lauritzen, et al., pp. 381–493, Springer-Verlag, Berlin Heidelberg.

Jansen, M., and R. Ferrari (2012), Macroturbulent equilibration in a thermally forced primitive equation system, *J. Atmos. Sci.*, *69*, 695–713.

Jansen, M. F., and I. M. Held (2014), Parameterizing subgrid-scale eddy effects using energetically consistent backscatter, *Ocean Modell.*, *80*, 36–48, doi:10.1016/j.ocemod.2014.06.002.

Jansen, M. F., I. M. Held, A. J. Adcroft, and R. Hallberg (2015), Energy budget-based backscatter in an eddy permitting primitive equation model. Submitted to *Ocean Modell.*

Killworth, P. D., and M. E. McIntyre (1985), Do Rossby-waves critical layers absorb, reflect or over-reflect?, *J. Fluid Mech.*, *161*, 449–492.

Kraucunas, I., and D. L. Hartmann (2005), Equatorial superrotation and the factors controlling the zonal-mean zonal winds in the tropical upper troposphere, *J. Atmos. Sci.*, *62*, 371–389.

Lapeyre, G., and I. M. Held (2003), Diffusivity, kinetic energy dissipation, and closure theories for the poleward eddy heat flux, *J. Atmos. Sci.*, *60*, 2907–2916.

Larichev, V. D., and I. M. Held (1995), Eddy amplitudes and fluxes in a homogeneous model of fully-developed baroclinic instability, *J. Phys. Oceanogr.*, *25*, 2285–2297.

Lauritzen, P., et al. (2014), A standard test case suite for two-dimensional linear transport on the sphere: Results from a collection of state-of-the-art schemes, *Geosci. Model Dev.*, *7*(1), 105–145.

Liu, Z., et al. (2009), Transient simulation of last deglaciation with a new mechanism for Blling-Allerd warming, *Science*, *325*, 310, doi: 10.1126/science.1171041.

Lorenz, D. (2014), Understanding midlatitude jet variability and change using Rossby wave chromatography: Wave-mean flow interaction, *J. Atmos. Sci.*, *71*, 3684–3705.

Lorenz, D., and D. Hartmann (2001), Eddy-zonal flow feedback in the Southern Hemisphere, *J. Atmos. Sci.*, *58*, 3312–3327.

Lorenz, E. N. (1967), *The Nature and Theory of the General Circulation of the Atmosphere*., 161 pp., World Meteorological Organization, Geneva.

Lutsko, N. J., I. M. Held, and P. Zurita-Gotor (2015), Applying the fluctuation-dissipation theorem to a two-layer Model of Quasi-Geostrophic Turbulence, *J. Atmos. Sci.*, *72*, in press.

MacVean, M. (1983), The effects of horizontal diffusion on baroclinic development in a spectral model, *Quarterly Journal of the Royal Meteorological Society*, *109*(462), 771–783.

Montoya, M., A. Griesel, A. Levermann, J. Mignot, M. Hofmann, A. Ganopolski, and S. Rahmstorf (2005), The earth system model of intermediate complexity CLIMBER-3. Part I: Description and performance for present day conditions, *Clim. Dyn.*, *25*, 237–263.

Peixoto, J. P., and A. H. Oort (1992), *Physics of Climate*, Am. Inst. of Phys., N. Y.

Pope, V., and R. Stratton (2002), The processes governing horizontal resolution sensitivity in a climate model, *Clim. Dyn.*, *19*, 211–236.

Ring, M. J., and R. A. Plumb (2008), The response of a simplified GCM to axisymmetric forcings: Applicability of the fluctuation-dissipation theorem, *J. Atmos. Sci.*, *65*, 3830–3898.

Sanchez, C., K. D. Williams, G. J. Shutts, R. E. McDonald, T. J. Hinton, C. A. Senior, and N. Wood (2013), Towards the development of a robust model hierarchy: Investigation of dynamical limitations at low resolution and possible solutions, *Q. J. R. Meteorol. Soc.*, *139*(670), 75–84.

Sanchez, C., K. D. Williams, G. Shutts, and M. Collins (2014), Impact of a stochastic kinetic energy backscatter scheme across time-scales and resolutions, *Q. J. R. Meteorol. Soc.*, *140*(685), 2625–2637.

Sato, T., H. Miura, M. Satoh, Y. N. Takayabu, and Y. Wang (2009), Diurnal cycle of precipitation in the tropics simulated in a global cloud-resolving model, *J. Clim.*, *22*, 4809–4826, doi:10.1175/2009JCLI2890.1.

Schneider, T., and C. C. Walker (2006), Self-organization of atmospheric macroturbulence into critical states of weak nonlinear eddy-eddy interactions, *J. Atmos. Sci.*, *63*, 1569–1586.

Shaffrey, L. C., et al. (2009), U.K. HiGEM: The new U.K. High-Resolution Global Environment ModelModel description and basic evaluation, *J. Clim. 22*, 1861–1896.

Shields, C. A., D. A. Bailey, G. Danabasoglu, M. Jochum, T. Kiehl, S. Leves, and S. Park (2012), The low-resolution CCSM4, *J. Clim.*, *25*, 3993–4014, doi:10.1175/JCLI-D-11-00260.1.

Shutts, G. (2005), A kinetic energy backscatter algorithm for use in ensemble prediction systems, *Q. J. R. Meteorol. Soc.*, *131*(612), 3079–3102.

Shutts, G. (2013), Coarse graining the vorticity equation in the ecmwf integrated forecasting system: The search for kinetic energy backscatter, *J. Atmos. Sci.*, *70*(4), 1233–1241.

Smith, R. S., and J. Gregory (2012), The last glacial cycle: Transient simulations with an AOGCM, *Clim. Dyn.*, *38*, 1545–1559, doi:10.1007/s00382-011-1283-y.

Steinhoff, J., and D. Underhill (1994), Modification of the Euler equations for vorticity confinement: Application to the computation of interacting vortex rings, *Phys. Fluids*, *6*(8), 2738–2744.

Tennant, W. J., G. J. Shutts, A. Arribas, and S. A. Thompson (2011), Using a stochastic kinetic energy backscatter scheme to improve mogreps probabilistic forecast skill, *Mon. Weather Rev.*, *139*(4), 1190–1206.

Thuburn, J., J. Kent, and N. Wood (2014), Cascades, backscatter and conservation in numerical models of two-dimensional turbulence, *Q. J. R. Meteorol. Soc.*, *140*, 626–638.

Timm, O., and A. Timmerman (2007), Simulation of the last 21 000 years using accelerated transient boundary conditions, *J. Clim.*, *20*, 4377–4401, doi:10.1175/JCLI4237.1.

Wan, H., M. Giorgetta, and L. Bonaventura (2008), Ensemble HeldSuarez test with a spectral transform model: Variability, sensitivity, and convergence, *Mon. Weather Rev.*, *136*, 1075–1092.

Williamson, D. (1999), Convergence of atmospheric simulations with increasing horizontal resolution and fixed forcing scales, *Tellus, Ser. A*, *51*, 663–673.

Zurita-Gotor, P., J. Blanco-Fuentes, and E. P. Gerber (2014), The impact of baroclinic eddy feedback on the persistence of jet variability in the two-layer model, *J. Atmos. Sci.*, *71*, 410–429.